Molecular Neurobiology (2019) 56:6952–6963
https://doi.org/10.1007/s12035-019-1575-5

Klotho-Mediated Changes in Shelterin Complex Promote Cytotoxic Autophagy and Apoptosis in Amitriptyline-Treated Hippocampal Neuronal Cells

Jennifer Mytych[1] · Przemyslaw Solek[1] · Anna Tabecka-Lonczynska[1] · Marek Koziorowski[1]

Received: 11 November 2018 / Accepted: 20 March 2019 / Published online: 3 April 2019

Abstract

Amitriptyline, antidepressant frequently prescribed for treatment of depressive disorders and several neuropathic and inflammatory diseases, has been shown to cause neurotoxic effects. This effect has been partially linked with increased oxidative stress and apoptosis initiation; however, the exact mechanism is still unknown. Klotho protein due to its neuroprotective characteristics seems to be involved in the amitriptyline-mediated neurotoxicity. In this study, we have evaluated the effect of *klotho* silencing on mouse hippocampal cells exposed to amitriptyline. We show, for the first time, that *klotho* silencing intensified in hippocampal neurons amitriptyline-induced imbalance in oxido-nitrosative and mineral homeostasis, genomic instability associated with telomere dysfunction what resulted in p16- and p53/p21-mediated cell cycle arrest and activation of autophagy and apoptotic cell death in consequence. Therefore, these results indicate that klotho serves as a part of the cellular defense mechanism engaged in the protection of neurons against amitriptyline-mediated toxicity.

Keywords Klotho · Amitriptyline · Telomeres · Autophagy · Apoptosis · Hippocampal cells

Introduction

Amitriptyline is a tricyclic antidepressant (TCA) frequently prescribed for treatment of depressive disorders and several neuropathic and inflammatory diseases, such as fibromyalgia, chronic fatigue syndrome, migraine, irritable bowel syndrome, and atypical facial pain [1]. On the other hand, amitriptyline has been shown to cause neurotoxic effects in vivo leading to neuronal and glial degeneration in the rodent model [2]. Several other reports, attempting to reveal the molecular mechanism underlying amitriptyline-mediated toxicity, have demonstrated that amitriptyline exerts toxic effects on the cellular level, through an increase in oxidative stress in cells of different types [1, 3–6], while dose-dependent neurotoxic properties of amitriptyline are linked, at least partially, with a loss of mitochondrial membrane potential, release of cytochrome c into the cytoplasm, activation of caspase 3 and, finally, initiation of apoptotic cell death [7, 8]. Furthermore, amitriptyline-mediated DNA damage [9], structural chromosomal abnormalities [10], and telomeres shortening [11] may be involved in the activation of neuronal apoptosis. However, the data is still fragmentary, and further studies are needed to evaluate the exact mechanism and factors involved in amitriptyline-induced neurotoxicity to ensure the reduction in TCA neurotoxic side effects and their safer clinical application.

Recent studies suggest that the anti-aging protein klotho exerts neuroprotective effects against neuronal injury associated with oxidative stress–mediated neurodegeneration. Klotho-deficient mice present with a reduced number of synapses, disrupted axonal transport, and a neurodegenerative phenotype in hippocampal pyramidal cells. On the other hand, mice overexpressing klotho exhibit long-term potentiation, and enhanced cognition, learning, and memory [12, 13]. Furthermore, pretreatment of in vitro hippocampal neurons with the recombinant klotho protects these cells from glutamate- and oligomeric amyloid β-induced cytotoxicity through the Akt-dependent modulation of the thioredoxin/peroxiredoxin system, an important contributor to neuronal

Electronic supplementary material The online version of this article (https://doi.org/10.1007/s12035-019-1575-5) contains supplementary material, which is available to authorized users.

✉ Jennifer Mytych
jennifermytych@gmail.com

[1] Department of Animal Physiology and Reproduction, Faculty of Biotechnology, University of Rzeszow, Werynia 502, 36-100 Kolbuszowa, Poland

antioxidant defense [14]. Taken together, klotho's ability to suppress oxidative damage–mediated apoptosis, and its crucial role in cognitive function, led us to hypothesize that klotho could be involved in the amitriptyline-induced neurotoxicity.

Therefore, the purpose of this study was to determine the effect of *klotho* silencing on mouse hippocampal cells (as in the brain klotho protein is mainly expressed by the choroid plexus and by neurons, especially in the hippocampus and the pituitary [15]) exposed to amitriptyline. This study will bring new important insight into mechanisms of neurotoxicity, emerging clinical issues linked with antidepressant treatment.

Materials and Methods

Materials

All reagents were of analytical grade purity and, unless stated otherwise, were purchased from Sigma. Antibodies' catalog numbers and their RRIDs are presented in the supplement.

Cell Culture, siRNA Transfection, and Amitriptyline Treatment

Mouse hippocampal neuronal cells, HT22 cell line (ATCC), were cultivated and maintained in a humidified atmosphere, at 37 °C, in the presence of 5% CO_2 in DMEM with 4.5 g/L glucose and 1 mM sodium pyruvate (without L-glutamine), supplemented with 10% fetal bovine serum (FBS) and an antibiotic mix solution (100 U/mL penicillin, 0.1 mg/mL streptomycin, 29.2 mg/mL L-glutamine). Typically, cells were passaged every 3 days by trypsinization. For siRNA transfection, cells were seeded into 12-well plates at the constant density of 7.5×10^3 cells/cm^2. After 24 h, cells were transfected with 10 pmol Ctrl-siRNA (Silencer Negative Control No. 1 siRNA; #AM4611, Thermo Scientific) or 10 pmol KLTH-siRNA (UniGeneID Hs.524953; siRNA ID 15391; #AM16708, Thermo Scientific–siRNA #1; UniGeneID Hs.524953; siRNA ID 15204; #AM16706, Thermo Scientific–siRNA #2) using 3 μL of Lipofectamine RNAiMAX reagent (Thermo Scientific) and following a standard manufacturer's protocol. The transfection efficiency was controlled after 48 h using the Western Blot method. For further experiments, 48 h after transfection, cells were trypsinized and seeded at the density of 3×10^3 cells/cm^2 and after 24 h treated with 10 μM amitriptyline (Cayman Chemical, stock prepared in DMSO). Cells were incubated with amitriptyline for 48 h and then following experiments were performed.

Cellular Oxidative and Nitrosative Stress Parameters

Measurements of intracellular superoxide anion (O2•-), nitric oxide (NO), and reduced glutathione levels (Thiol) were performed according to manufacturers' protocols, using fluorogenic redox-sensitive probes: dihydroethidium (Thermo Scientific), 4-amino-5-methylamino-2′,7′-difluorofluorescein diacetate (Cayman Chemicals), and Thiol Tracker Violet (Thermo Scientific), respectively. Digital photographs were captured with InCell Analyzer 2000 equipped with InCell Analyzer 2000 Software. A minimum of 1000 cells were counted in each sample, and quantifications results were presented as relative fluorescence units (RFU).

Intracellular Zinc and Calcium Levels Detection

After trypsinization, cells were suspended in HBSS at the density of 2×10^5 cells/mL and one of the fluorescent probes (Zinquil ethyl ester for zinc (Zn^{2+}) or Fura-PE3AM for calcium (Ca^{2+}) detection, Cayman Chemical) at the final concentration of 2 μM was added. Cells were incubated for 15 min at 37 °C and fluorescence intensity was measured in a microplate reader PerkinElmer Victor X4 2030 (λex = 368 nm, λem = 490 nm–Zinquin ethyl ester; 335 nm/364 nm ratio–Fura-PE3AM). Results are presented as % of control.

Western Blot Analysis

Western blot procedure was previously described in Mytych et al. [16]. Briefly, 30 μg of protein lysates prepared in ice-cold RIPA buffer were separated by 10% SDS-PAGE, electroblotted to PVDF membranes, blocked in 1% BSA, and incubated with specific primary and secondary HRP-conjugated antibodies. Protein bands were visualized using Clarity Max Western ECL Substrate (BioRad) and the Fusion Fx7 system. The relative protein expression levels were normalized to β-actin (GelQuantNET software).

Immunostaining

For immunostaining, a standard protocol reported in previous studies was employed [16, 17]. Briefly, cells were washed twice with PBS, fixed for 15 min in 4% paraformaldehyde, permeabilized for 20 min with PBS-T (PBS with 0.25% Triton-X), blocked with 1% BSA, and incubated overnight with a relevant primary antibody diluted in the blocking buffer. Then, cells were washed twice in PBS-T and incubated for 1 h with secondary antibody conjugated with a fluorochrome. Nuclei were visualized with Hoechst 33258. Digital images were captured with InCell Analyzer 2000 and analyzed with ImageJ. A minimum of 1000 cells were counted in each sample and results for H2A.X and LC3 immunostaining are

presented as puncta/cells. For BrdU immunostaining, 10 μM BrdU were added to cells 6 h before fixation. Then, the procedure was continued as described above with one modification. After permeabilization, cells were denatured with 2 M HCl at 37 °C for 60 min to unfold DNA strands and allow antibodies to bind to incorporated BrdU. Positive cells were counted and presented as %, while the results obtained for the control were considered as 100%.

Cell Cycle and Micronuclei Formation Analysis

Photographs taken after nuclei visualization with Hoechst 33258 during immunostaining protocols were used for cell cycle status assessment. The cell cycle profile was evaluated using DNA Cell cycle plug-in from ImageJ software and results are presented as % of cells in each of G0/G1, S, and G2/M phases. Chromosomal DNA damage in cells in response to the genotoxic compound was estimated using the InCell Analyzer 2000 micronuclei formation analysis module. The analysis was performed on digital images taken after cell cycle assessment. A minimum of 1000 cells were automatically counted in each sample improving a statistical reliability of the results.

Reverse Transcribed PCR

Total RNA was extracted with Trizol reagent according to the manufacturer's protocol (Thermo Scientific) and 2 μg of RNA were reverse transcribed to cDNA, using High-Capacity cDNA Reverse Transcription Kit (Thermo Scientific). Furthermore, the reaction mixture for each PCR analysis contained 5 μl of 2xPCR TaqNova-RED Master Mix (DNA Gdansk), 4 μl of primers (2 μl of each 1 μM forward and reverse primer, GenoMed), and 1 μl of cDNA (10 ng). The PCR reactions were conducted for 35 denaturing cycles at 95 °C for 45 s, annealing at the temperature designated for each primer pair (Table 1) for 45 s, followed by extension at 72 °C for 45 s, and final extension at 72 °C for 10 min. Telomere length was verified by PCR and specific primers, according to the methodological paper published by O'Callaghan et al. [18]. PCR products were electrophoretically detected on 1.5% agarose gel after ethidium bromide staining, using the Fusion Fx7 system. The optical density was calculated using GelQuantNET software, numerically expressed as the relative density normalized to the β-actin expression level.

MTT Test

The MTT assay was performed according to the standard protocol described previously [19]. Briefly, after incubation, 500 μg/mL MTT were added to the medium. After 4 h incubation at 37 °C, the medium was discarded, crystals were dissolved in DMSO, and absorbance was read with a microplate reader Victor X4 (570 nm and 630 nm, measurement and reference wavelengths, respectively). The results are presented as %, while readings for the untreated control are considered as 100%.

ATP Level Determination

ATP levels were measured using ATPlite Luminescence Assay (PerkinElmer) according to the manufacturer's instructions. Briefly, the cell culture medium was removed and cells were lysed with a lysis solution. Then, the substrate solution was added, and the luminescent signal was monitored in a microplate reader Victor X4. The results are presented as relative luminescent units (RLU).

Morphological Analysis

The morphology of cells was visualized with Tubulin Tracker fluorescent dye (Thermo Scientific). The cell culture medium was removed, and the cells were rinsed twice with HBSS solution and covered with the 50 nM staining solution prepared in HBSS. The cells were incubated at 37 °C for 30 min, rinsed twice with HBSS, and immediately photographed with InCell Analyzer 2000.

Acridine Orange Staining

To visualize autophagosomes, cells were covered with 1 μg/mL acridine orange (AO) solution prepared in DMEM at 37 °C for 15 min. After incubation, the staining solution was removed and the cells were washed twice with PBS. Digital images were taken with InCell Analyzer 2000, analyzed with InCell Analyzer analysis module and presented as relative fluorescence units. A minimum of 1000 cells were counted in each sample.

Statistical Analysis

All data are expressed as the mean ± standard deviation of three independent experiments. The statistical analysis of the results was performed using GraphPad Prism ver. 6.0. Differences between the control and the test samples were assessed with the one-way ANOVA followed by Dunnett's multiple comparison post-test. A p value of < 0.05 was considered as statistically significant (***/^^^$p < 0.001$; **/^^$p < 0.01$; */^$p < 0.05$, no indication–no statistical significance). (*) indicates a comparison between AMI-untreated and treated Ctrl-siRNA or KLTH-siRNA cells, (^) indicates a comparison between AMI non-treated Ctrl-siRNA and KLTH-siRNA cells, or AMI-treated Ctrl-siRNA and KLTH-siRNA cells.

Table 1 Primers sequences used in this study

Gene	Primer sequence	Annealing temp. (°C)
TRF1	fwd: TTCCCGAAAGTGGTGGAGTTT rev: TGGCCTTTAGGCTCATACACA	62
TRF2	fwd: CCTCCCAGAAACTCAAGCGG rev: TCTCGTCAACCACAATCTCCT	63
RAP1	fwd: TTCTTTACCAAATTGTGGTGGCT rev: CTCCGACTTGTAGGCTGTGG	62
TPP1	fwd: GGCAAATGCACTTACAACCCT rev: CTCCGAGAGTCTTTCCAGGT	61
TIN2	fwd: AAGAGCATGACCGTCCTCCT rev: GGGTGGTGTACTTAGTGTCCTC	63
POT1	fwd: TTGGTTTCAACAGCTCCCTATAC rev: GGAGGGCTTCATAGTTTCCACT	62
TELO	fwd: CGGTTTGTTTGGGTTTGGGTTTGGGTTTGGGTTTGGGTT rev: GGCTTGCCTTACCCTTACCCTTACCCTTACCCTTACCCT	72
ACTB	fwd: GCAGGAGTACGATGAGTCCG rev: ACGCAGCTCAGTAACAGTCC	68

Results

Klotho Silencing Sensitizes Hippocampal Cells to Amitriptyline Treatment

We decided to use the siRNA strategy to silence *klotho* expression, and to verify the role of klotho protein in hippocampal cells during amitriptyline treatment. In this study, we used two different siRNAs to target *klotho*. As expected, cells treated with KLTH-siRNAs exhibited a decreased level of klotho protein synthesis; however, its efficiency varied, as shown in Fig. 1. Western blot analysis revealed that the expression of the transmembrane form of klotho of a molecular weight of 130 kDa dropped by 66.43% in cells transfected with #2 KLTH-siRNA, when compared to cells treated with the negative control siRNA (Ctrl-siRNA) ($p < 0.001$). Simultaneously, the level of the secreted form of the klotho protein (65 kDa) dropped by 57.01% ($p < 0.01$). On the other hand, transfection with #2 KLTH-siRNA reduced the level of transmembrane klotho by 11.75%, and of the secreted form, by 6.94% (Fig. 1). Thus, we decided to continue the study using more efficient KLTH-siRNA, i.e., #2.

It was already demonstrated that klotho increases resistance to oxidative stress; therefore, when the HT-22 model with silenced klotho was established, we decided to verify whether klotho protein was engaged in maintaining redox and mineral homeostasis during amitriptyline treatment. Thus, we analyzed the phenotype of Ctrl-siRNA and KLTH-depleted cells in two experimental conditions, control (w/o amitriptyline treatment) and upon stimulation with 10 μM amitriptyline for 48 h. Interestingly, incubation of the KLTH-cells with amitriptyline led to a 1.44-fold increase in intracellular superoxide generation ($p < 0.01$), while Ctrl-siRNA cells remained unaffected (Fig. 2a). Similarly, amitriptyline treatment resulted in the change in the intracellular pool of nitric oxide, however, only in KLTH-siRNA cells. When compared to control, a 1.32-fold decrease in NO production was noted in KLTH-siRNA cells ($p < 0.01$) (Fig. 2b). The maintained oxido-

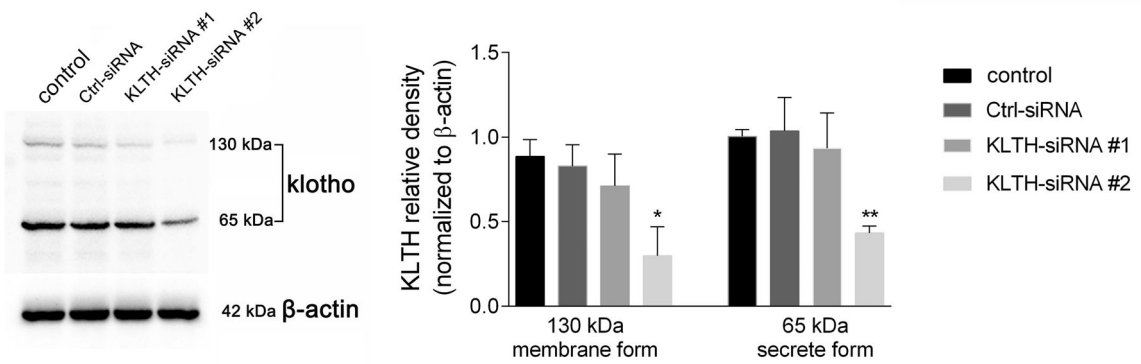

Fig. 1 siRNA-mediated *klotho* silencing of mouse hippocampal cells (HT22 cell line). Cells were transfected with 10 pmol Silencer Negative Control (Ctrl-siRNA) or 10 pmol klotho siRNA (KLTH-siRNA #1 and #2) for 48 h and western blot analysis of klotho membrane (130 kDa) and secrete (65 kDa) form expression was performed. Bars indicate SD, $n = 3$, $^{**}p < 0.01$, $^{*}p < 0.05$ (one-way ANOVA and Dunnett's a posteriori test)

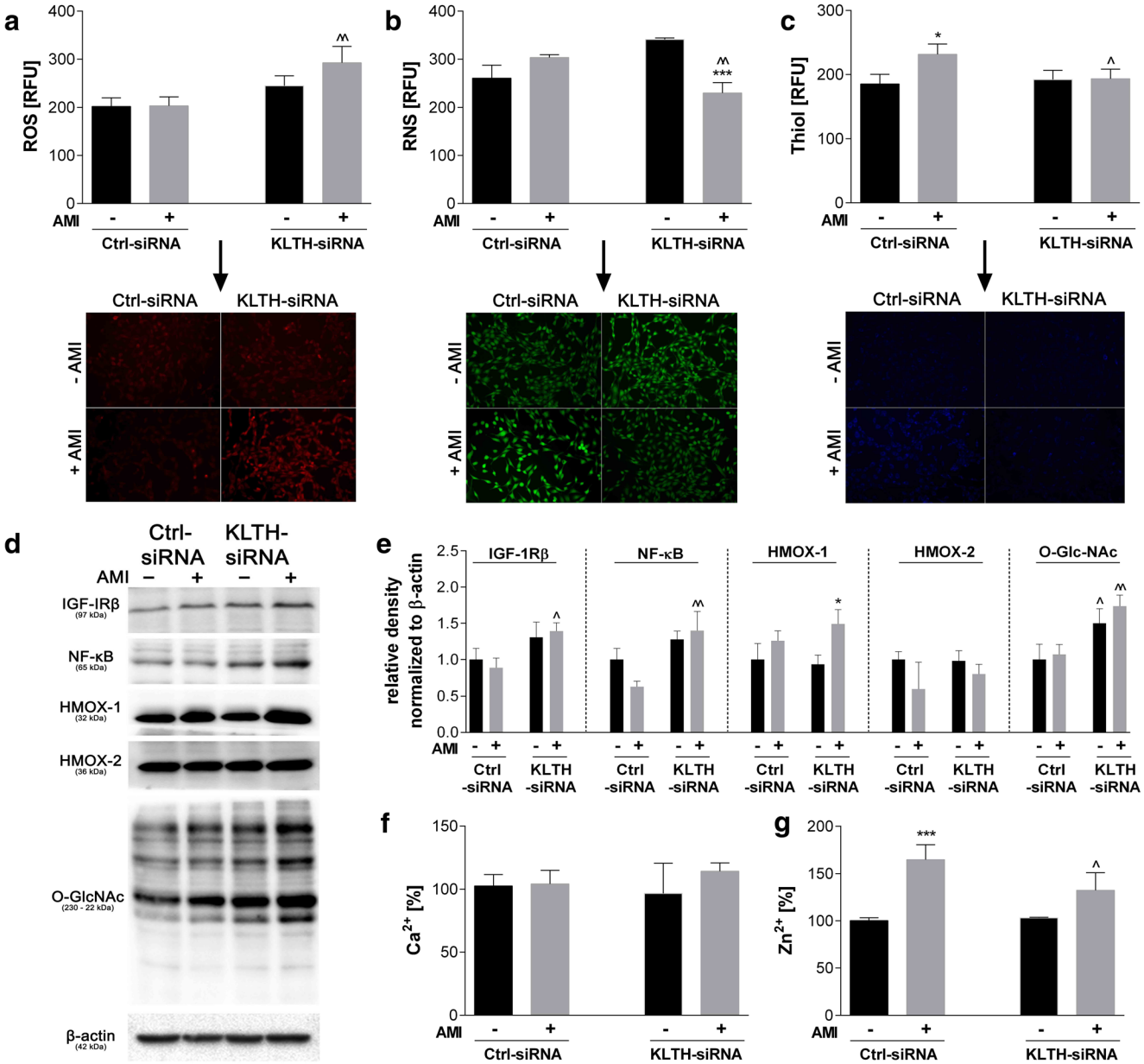

Fig. 2 *Klotho* depletion increases oxidative/nitrosative stress and leads to an imbalance in intracellular zinc and calcium homeostasis. After transfection, cells were treated for 48 h with 10 μM amitriptyline and **a** reactive oxygen species, **b** nitric oxide, **c** thiol, **d-e** activation of antioxidant pathways and extent of O-GlcNAcylation, **f** Ca^{2+}, **g** Zn^{2+} levels were measured. Red fluorescence–dihydroethidium (ROS), green–4-amino-5-methylamino-2′,7′-difluorofluorescein diacetate (NO), blue fluorescence–Thiol Tracker (Thiol). Magnification of the objective lens × 10. Bars indicate SD, $n = 3$, ***/^^^$p < 0.001$, **/^^$p < 0.01$, */^$p < 0.05$, no indication–no statistical significance (one-way ANOVA and Dunnett's a posteriori test). (*) indicate comparison between AMI-non-treated and treated Ctrl-siRNA or KLTH-siRNA cells, (^) indicate comparison between AMI non-treated Ctrl-siRNA and KLTH-siRNA cells or AMI-treated Ctrl-siRNA and KLTH-siRNA cells

nitrosative balance in the Ctrl-siRNA cells resulted from activation of the adaptive response involving the glutathione antioxidant system, as manifested by upregulation of the thiol pool (Fig. 2c). The level of thiols, reflecting a reduced glutathione content in the Ctrl-siRNA cells increased by approximately 25% ($p < 0.05$). At the same time, the cells with silenced *klotho* expression did not exhibit any changes in thiols level (Fig. 2c). On the other hand, amitriptyline treatment promoted activation of IGF-IR ($p < 0.05$) and NF-κB transcription factor ($p < 0.01$) pathways only in KLTH-siRNA cells. In consequence, the level of heme oxygenase 1 (HMOX-1) was also elevated ($p < 0.05$); however, the expression of constitutive heme oxygenase 2 (HMOX-2) remained essentially unchanged. Furthermore, *klotho* silencing led to increased protein O-GlcNAcylation, and amitriptyline treatment even resulted in the observed 1.61-fold rise ($p < 0.01$) (Fig. 2d–e). As mineral imbalance is inseparably linked to oxido-nitrosative stress, in the next step of this study, we

decided to control amitriptyline-mediated changes in intracellular levels of calcium and zinc ions. While Ca^{2+} pools were unaffected in all experimental set-ups analyzed (Fig. 2f), Zn^{2+} levels were upregulated in Ctrl-siRNA but not in KLTH-siRNA cells as a consequence of amitriptyline treatment ($p < 0.001$) (Fig. 2g).

Klotho Depletion Affects Genomic Stability During Amitriptyline Stimulation

Reactive oxygen species are known to contribute to DNA lesions and breaks. Also, mitochondria, sensors, and regulators of calcium and zinc signaling are most likely the major source of ROS. In this study, we observed disrupted oxidative and mineral homeostasis; thus, we decided to investigate possible DNA damage resulting from amitriptyline treatment in *klotho*-silenced cells. Western blot analyses confirmed that in the KLTH-depleted cells, amitriptyline treatment led to a 1.54-, 2.04-, and 1.92-fold increase in the levels of p16 ($p < 0.05$), p21 ($p < 0.01$), and p53 ($p < 0.05$) proteins, respectively. A similar tendency was not observed in the cells transfected with Ctrl-siRNA. The same analysis revealed that the levels of p27 protein remained unaffected in all conditions analyzed (Fig. 3a–b). This confirmed that amitriptyline stimulation activates p53/p21- and p16-dependent DNA damage response (DDR) pathways in the KLTH-siRNA cells. As further revealed, DDR activation occurred as the consequence of DNA breaks. A 2.06-fold increase in DNA double–strand breaks was observed in the amitriptyline-treated KLTH-siRNA cells, as assessed by γH2A.X foci formation analysis, when compared to the Ctrl-siRNA cells ($p < 0.01$) (Fig. 3c). Simultaneously, we confirmed increased micronuclei formation in the amitriptyline-treated KLTH-siRNA cells, when compared to the Ctrl-siRNA cells, with the noted upregulation of 57% ($p < 0.05$) (Fig. 3d). Moreover, a detailed analysis of γH2A.X immunostaining photographs revealed that the overwhelming majority of γH2A.X foci were located in formed micronuclei (Fig. 3e).

Klotho Depletion Affects Shelterin Complex During Amitriptyline Stimulation

Development of nuclear anomalies, such as micronuclei, is mainly caused by chromosome instability related to telomeres [20]. Also, activation of the p53/p21 pathway, observed in this study, is closely associated with telomere dysfunction. Thus, we decided to control the components of the telomeric complex, as well as telomere length. We started with verifying expression of six genes (*POT1*, *TRF1*, *TRF2*, *TPP1*, *TIN2*, and *RAP1*) involved in the formation of a so-called shelterin complex known to be crucial for both maintenance of telomere structure and their signaling functions. In the Ctrl-siRNA cells, amitriptyline treatment did not affect their expression profile. Similarly, expression of *POT1* and *RAP1* remained unchanged in the KLTH-siRNA cells, even after incubation with amitriptyline. However, when the amitriptyline-treated

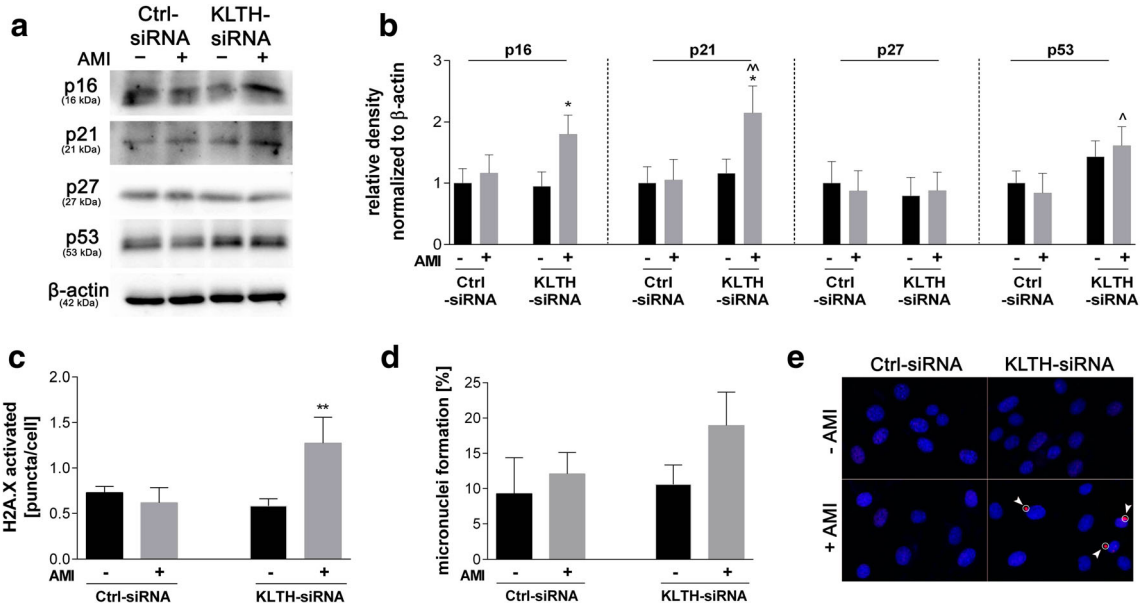

Fig. 3 *Klotho* silencing increases AMI-mediated DNA damage and leads to cell cycle arrest. After transfection, cells were treated for 48 h with 10 μM amitriptyline and **a**–**b** AMI-mediated changes in the expression of proteins involved in cell cycle control, **c** γH2A.X, and **d** micronuclei formation were monitored; **e** representative images are presented. Blue fluorescence–Hoechst 33258 (nuclei), red fluorescence–PECy5. Magnification of the objective lens × 20. Bars indicate SD, $n = 3$, **/^^$p < 0.01$, */^$p < 0.05$, no indication–no statistical significance (one-way ANOVA and Dunnett's a posteriori test). (*) indicate comparison between AMI-non-treated and treated Ctrl-siRNA or KLTH-siRNA cells, (^) indicate comparison between AMI-non-treated Ctrl-siRNA and KLTH-siRNA cells or AMI-treated Ctrl-siRNA and KLTH-siRNA cells

Ctrl-siRNA and KLTH-siRNA cells were compared, statistically significant downregulation of *TRF1* ($p < 0.05$), *TRF2* ($p < 0.01$), *TIN2* ($p < 0.001$), and *TPP1* ($p < 0.05$) expression was observed in KLTH-depleted cells. Interestingly, *klotho* silencing resulted in upregulated *TIN2* expression in the untreated HT-22 cells. Although the expression of genes associated with the shelterin complex was disrupted in the KLTH-siRNA cells treated with amitriptyline, the length of their telomeres remained unaffected when compared to the control cells (Fig. 4). However, this may result from the short duration of the experiment.

Activation of Cytotoxic Autophagy and Apoptotic Cell Death in Amitriptyline-Treated Klotho-Depleted Cells

In KLTH-siRNA cells treated with amitriptyline, telomere instability and DNA damage, consequences of oxidative stress, and nitrosative homeostasis imbalance resulted in activation of the p53/p21- and p16-mediated DDR pathways. The cell cycle arrest in G2/M phase was activated, allowing cells to repair critical damage. The percentage of the KLTH-siRNA cells in G2/M phase increased by 14.6% when compared to the Ctrl-siRNA cells ($p < 0.01$). Also, a slight but statistically significant decrease in the pool of cells in S phase was noted ($p < 0.05$) (Fig. 5a). This data was supported by results obtained in the BrdU incorporation test. Additionally, amitriptyline-mediated downregulation of the Ctrl-siRNA cells proliferation rate was also observed, but to a lesser extent (Fig. 5b). Amitriptyline treatment resulted in downregulation of mitochondrial respiration in both Ctrl-siRNA and KLTH-siRNA cells; however, that effect was more pronounced in the KLTH-siRNA cells ($p < 0.001$) (Fig. 5c). This was probably due to the decreased number of cells and the reduced proliferation rate, since ATP level was maintained in all experimental set-ups analyzed (Fig. 5d). Furthermore, tubulin staining not only confirmed the reduction in the number of cells, but also

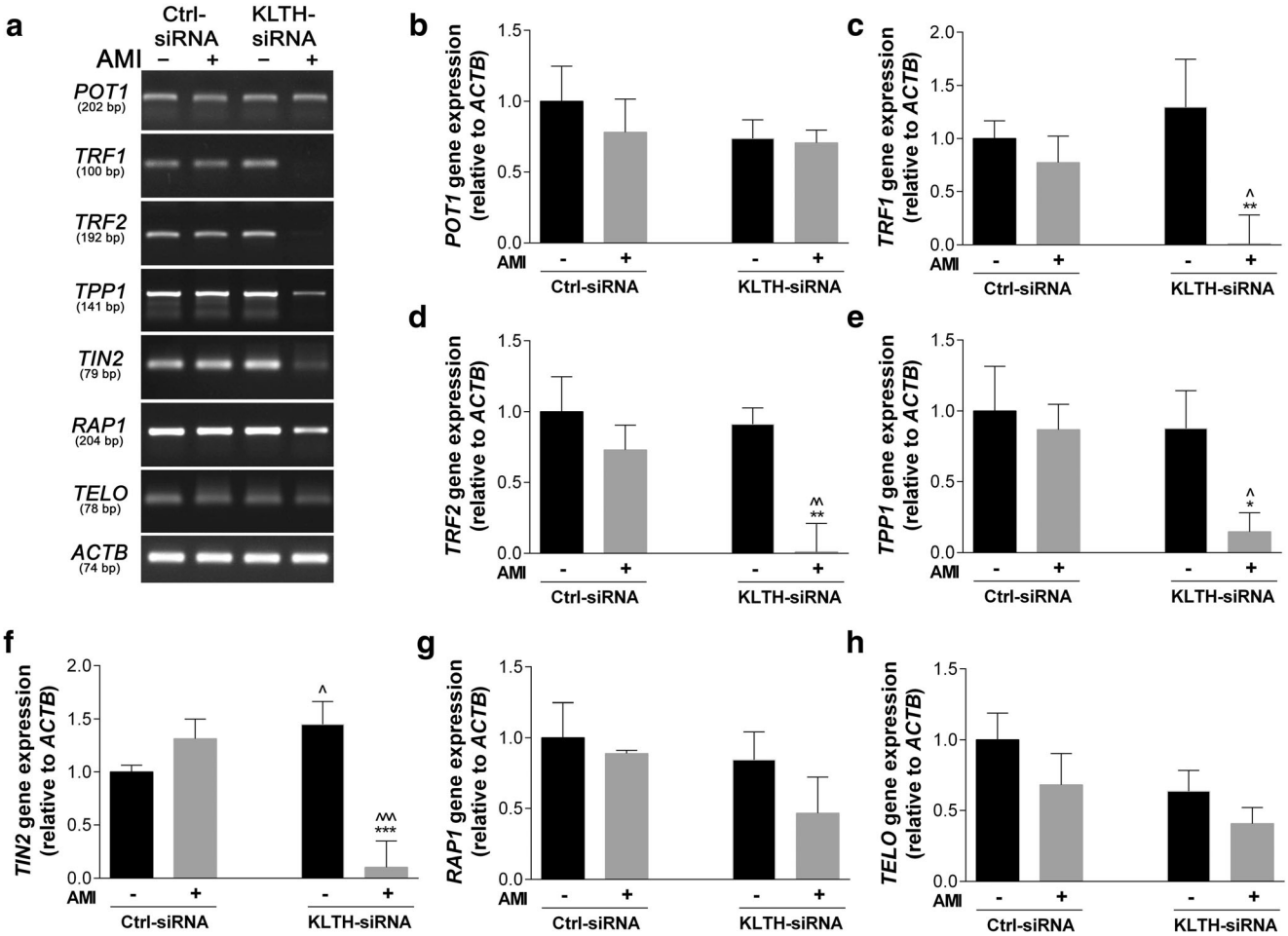

Fig. 4 *Klotho* siRNA affects the expression of **a** telomeric complex components during amitriptyline challenge. After transfection, cells were treated for 48 h with 10 μM amitriptyline and expression of **b** *POT1*, **c** *TRF1*, **d** *TRF2*, **e** *TPP1*, **f** *TIN2*, and **g** *RAP1* genes as well as **h** telomere length were monitored. Representative bands are presented. Bars indicate SD, $n = 3$, ***/^^^$p < 0.001$, **/^^$p < 0.01$, */^$p < 0.05$, no indication–no statistical significance (one-way ANOVA and Dunnett's a posteriori test). (*) indicate comparison between AMI-non-treated and treated Ctrl-siRNA or KLTH-siRNA cells, (^) indicate comparison between AMI non-treated Ctrl-siRNA and KLTH-siRNA cells or AMI-treated Ctrl-siRNA and KLTH-siRNA cells

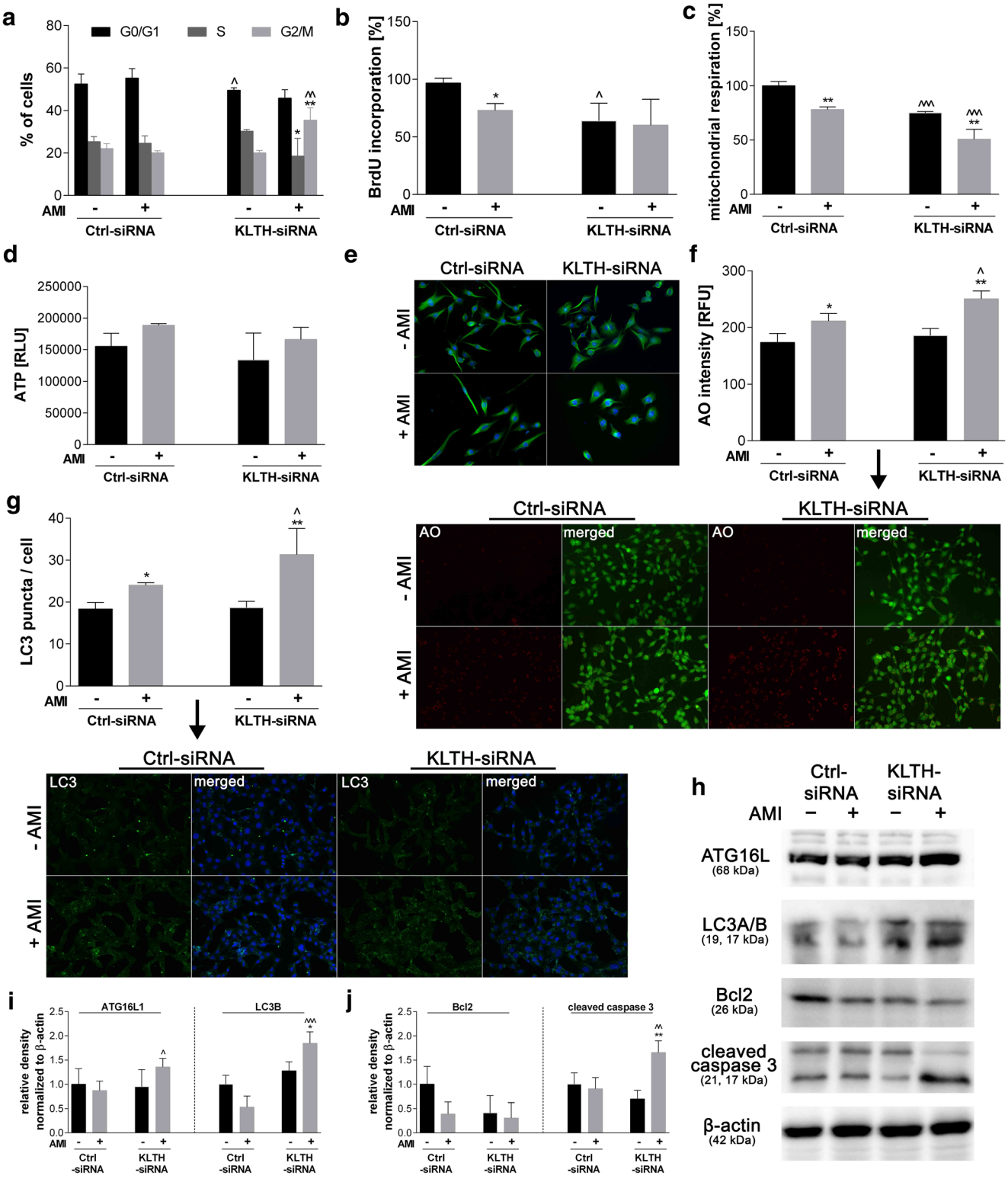

revealed substantial changes in cell morphology. Despite amitriptyline treatment, the Ctrl-siRNA cells preserved morphological features and functional characteristics of the HT-22 cells. At the same time, the amitriptyline-treated KLTH-siRNA cells became enlarged, flattened, and disorganized (Fig. 5e). Together with G2/M cell cycle arrest, those morphological changes may also suggest activation of autophagy, and further experiments confirmed this theory. In the Ctrl-siRNA

◀ **Fig. 5** *Klotho* depletion leads to activation of cytotoxic autophagy and apoptotic cell death in amitriptyline-treated cells. After transfection, cells were treated for 48 h with 10 μM amitriptyline and **a** cell cycle progression, **b** BrdU incorporation, **c** mitochondrial respiration, **d** ATP level, **e** morphology, **f** acidic compartments presence–acridine orange (AO) staining, **g** LC3 puncta amount, and **h**–**j** expression of proteins involved in apoptosis and autophagy activation were controlled. Representative photos are presented. Blue fluorescence–Hoechst 33258 (nuclei); green fluorescence–Tubulin Tracker (**e**), orange acridine (AO) (**f**–cytoplasm), FITC (**g**); red fluorescence–orange acridine (AO) (**f**–acidic compartments). Magnification of the objective lens × 10 (**f, g**) and × 20 (**e**). Bars indicate SD, $n = 3$, ***/^^^$p < 0.001$, **/^^$p < 0.01$, */^$p < 0.05$, no indication–no statistical significance (one-way ANOVA and Dunnett's a posteriori test). (*) indicate comparison between AMI-non-treated and -treated Ctrl-siRNA or KLTH-siRNA cells, (^) indicate comparison between AMI-non-treated Ctrl-siRNA and KLTH-siRNA cells or AMI-treated Ctrl-siRNA and KLTH-siRNA cells

cells, we detected a 1.22-fold increase in acridine orange staining intensity, reflecting acidic compartments resulting from amitriptyline treatment ($p < 0.05$), while in the KLTH-siRNA cells, this effect was even intensified by another 1.18-fold increase ($p < 0.01$) (Fig. 5f). More specific method, i.e., LC3 immunostaining, revealed the same tendency. Amitriptyline treatment resulted in the 30.71% increase in LC3 puncta/cell presence in the Ctrl-siRNA cells, while in the KLTH-siRNA cells, 67.93% upregulation was observed ($p < 0.01$) (Fig. 5g). The Western blot analysis against the LC3A/B antibody confirmed these observations (Fig. 5h–i). The level of ATG16L, a protein crucial in autophagosome formation, was also elevated in the amitriptyline-treated KLTH-siRNA cells when compared to the Ctrl-siRNA cells (by approximately 56%) (Fig. 5h–i). Activation of autophagy may not only initiate restoration of cellular functions (protective autophagy), but also lead to cell death (cytotoxic autophagy). Therefore, we evaluated the levels of Bcl2 and active caspase 3, proteins involved in the apoptotic cell death mechanism. In contrast to the Ctrl-siRNA cells, the KLTH-siRNA cells treated with amitriptyline were characterized by significantly increased levels of active caspase 3 with a concomitant drop in the Bcl2 pool, confirming activation of apoptosis (Fig. 5h, j).

Discussion

Amitriptyline-induced neurotoxicity has already been confirmed in many studies [7, 8]; however, the exact molecular mechanisms underlying this process have not been fully understood yet. In this study, for the first time, we confirmed that amitriptyline induces mild stress–mediated activation of prosurvival protective autophagy in control hippocampal neurons. At the same time, *klotho* silencing results in significantly intensified oxidative stress–mediated DNA damage, and thus initiation of cytotoxic autophagy and apoptotic cell death. Additionally, we report the precise mechanism underlying these interactions.

Regulation of members of the redox system has already been linked to the neuroprotective effect of klotho. It was shown to be involved in the induction of Prx-2 expression, a key modulator of neuroprotection by inhibitory phosphorylation of the transcription factor forkhead box O3a (FoxO3a) [14]. Similarly, klotho prevents oxidant-induced degeneration of dopaminergic neurons by modulating ASK1 and p38 MAPK signaling pathways [21]. These characteristics are in agreement with our observations, where after amitriptyline treatment, *klotho* silencing intensified oxidative stress, as well as led to NF-κB and heme oxygenase 1 activation. This could be due to the direct interplay between reactive oxygen species and nitric oxide, as it was reported to lead to peroxynitrite formation, and thus, to the reduction in NO levels [22]. On the other hand, in neurons, peroxynitrite induces apoptosis by releasing zinc from intracellular stores [23], and this was also confirmed during our study. However, the reduction in NO pools may also be a consequence of klotho-mediated modulation of iNOS activity [24], which is particularly important in the nervous system, where NO plays a crucial role in synaptic plasticity and neurotransmission [25]. Furthermore, inhibition of AMI-mediated expression of NO in the *klotho*-deficient cells was associated with manifested enhanced O-GlcNAcylation. O-GlcNAcylation, as a dynamic post-translational modification, regulates a range of cellular processes, including stress response; nonetheless, its upregulated levels are associated with decreased proliferation, premature differentiation, and increased apoptosis in neural progenitors [26]. O-GlcNAcylation was also shown to protect genome integrity when the cell cycle is challenged by DNA damage stresses [27]. Thus, elevated levels of O-GlcNAcylation may indicate activation of the AMI-mediated stress response due to the DNA damage. Here, we confirmed that oxidative stress and mineral imbalance resulted in DNA damage in the *klotho*-depleted cells after amitriptyline treatment. In this study, DNA lesions were mostly located in telomeres, as validated by elevated levels of micronuclei formation and inhibition of the shelterin complex. At telomeres, the shelterin complex is constituted by a group of six proteins which assembles quantitatively along the telomere tract and imparts both telomere maintenance and telomere protection by strict coordination [28]. Disruption of the shelterin proteins or the telomere heterochromatic state was shown to induce de-protection of telomeres, resulting in telomere abnormalities recognized as damaged DNA. In this study, amitriptyline treatment was associated with decreased expression of 4 components of the shelterin complex (TRF1, TRF2, TIN2, and TPP1) in the *klotho*-silenced hippocampal cells, while RAP1 and POT1 levels remained unaffected. Inhibition of TRF2 is strictly linked with dysfunctional, uncapped telomeres, and was shown to be associated with several DNA damage response factors, including γH2AX and 53BP1 [29], similarly as observed in our study. Additionally, some co-localization occurs

between appearance of γH2AX foci and TRF1 reduction, and is defined as a marker of telomeric DNA damage. We also confirmed in this study that most of the γH2AX foci were located within formed micronuclei, and this also suggests telomeric DNA damage. Furthermore, there is evidence that oxidative stress induces 8-oxoG at telomeric sequences, leading to transversions of guanine-cytosine content to adenine-thymine content (A/T → G/C). Adenine, in turn, impedes binding of TRF1 and TRF2 to telomeres, and thus reduces their expression [30]. Additionally, downregulated levels of TRF1 and TRF2 may be a consequence of decreased TIN2 and TPP1 expression, since they serve as critical interconnectors of the shelterin complex [31]. Interestingly, despite disrupted formation of the shelterin complex, we did not confirm any changes in the telomere length. This could be due to the fact that experiments were conducted only for 48 h; therefore, the differences in the telomere lengths could remain undetected due to the limited number of proliferation cycles. On the other hand, as already mentioned, the POT1 levels were unaffected. Since POT1 appears to interact with telomeres through direct binding to the 3′ overhanging G-strand DNA or through interaction with the TRF1 duplex telomere DNA binding complex and is involved in telomere length regulation [32], it is likely that in this study it interacts independently of other components of the shelterin complex, and thus prevents telomeres from shortening. A sophisticated network of DNA damage response systems is activated to deal with DNA damage; however, it is well known that telomere damage is repaired less efficiently than the whole genome [30]. In this study, we confirmed that accumulated damage resulting from amitriptyline treatment leads to p16- and p53/p21-dependent arrest of the *klotho*-depleted cells in G2/M phase. This supports the theory that DNA damage occurring in telomere regions is often recognized in G2 phase of the cell cycle [33]. Despite the cell cycle arrest and time for repair, the damage is too severe and redirects cells to autophagy and apoptosis. Literature confirms that G2/M arrest can be followed either by autophagy, apoptosis, or autophagy along with apoptosis; however, the final fate of cells is determined by the result of cross-talk between apoptosis and autophagy. In addition, autophagy, although not leading to cell death by itself, can induce apoptosis by participating in apoptotic processes, such as ATP-dependent events and phosphatidylserine exposure and membrane blebbing [34]. On the other hand, in some instances, apoptosis is involved in autophagosome formation through the AMPK/RAPTOR/mTOR pathway [35]. Moreover, a basic or low-level autophagy allows cell survival during stress (prosurvival autophagy); however, intensive or prolonged autophagy results in cell death (cytotoxic autophagy) [36]. In this study, we observed both types of autophagy. Prosurvival autophagy was detected in the control (non-*klotho*-silenced) hippocampal cells treated with amitriptyline, where mild stress and zinc-induced autophagosome formation facilitated cell survival [37], as confirmed by acridine orange and LC3 puncta staining. In contrast, *klotho* depletion resulted in activation of both autophagy and apoptosis after amitriptyline treatment. Both processes are known to be initiated in response to unrepairable DNA damage. Apoptosis is a primary response to micronuclei induction in p53-competent cells such as murine hippocampal neurons [38]. On the other hand, autophagy is known as critical for efficient removal of double-strand DNA breaks [39], and γH2AX-positive immunostaining confirms this kind of DNA damage in the *klotho*-silenced cells treated with amitriptyline. Additionally, potent telomere damage through TRF2 delocalization from telomeres leads to autophagy [40]. It has already been demonstrated the amitriptyline-induced autophagy in primary astrocytes and neurons leads to decrease in viability, with neurons entering apoptosis [41]. However, in this study, we indicate the crucial role of the klotho protein in modulating this cross-talk through alteration in the shelterin complex.

In conclusion, in this study, for the first time, we show that in hippocampal neurons *klotho* silencing intensified amitriptyline-induced imbalance in oxido-nitrosative and mineral homeostasis and genomic instability associated with telomere dysfunctions leading to p16- and p53/p21-mediated cell cycle arrest and, in consequence, to activation of autophagy, as well as of apoptotic cell death. Therefore, these results indicate that klotho serves as a part of the cellular defense mechanism engaged in protection of neurons against amitriptyline-mediated toxicity.

Acknowledgements The authors would like to thank Slawomir Nowak, MSc, for providing antibodies against HMOX-1 and HMOX-2.

Authors' Contributions JM performed the experiments, analyzed the data, carried out data interpretation, wrote the paper, and conceived and designed the experiments. PS performed the experiments, analyzed the data, carried out data interpretation, and wrote the paper; AT-L performed the experiments. MK conceived and designed the experiments, and carried out data interpretation.

Funding This work was supported by the "Preludium" no. UMO-2014/15/N/NZ7/04097 funded by the Polish National Science Center.

Compliance with Ethical Standards

Conflict of Interest The authors declare that they have no competing interests.

References

1. Villanueva-Paz M, Cordero MD, Pavon AD, Vega BC, Cotan D, De la Mata M, Oropesa-Avila M, Alcocer-Gomez E et al (2016) Amitriptyline induces mitophagy that precedes apoptosis in human

HepG2 cells. Genes Cancer 7(7–8):260–277. https://doi.org/10.18632/genesandcancer.114
2. Sudoh Y, Desai SP, Haderer AE, Sudoh S, Gerner P, Anthony DC, De Girolami U, Wang GK (2004) Neurologic and histopathologic evaluation after high-volume intrathecal amitriptyline. Reg Anesth Pain Med 29(5):434–440
3. Karlsson H, Gu Y, DePierre J, Nassberger L (1998) Induction of apoptosis in proliferating lymphocytes by tricyclic antidepressants. Apoptosis 3(4):255–260
4. Viola G, Miolo G, Vedaldi D, Dall'Acqua F (2000) In vitro studies of the phototoxic potential of the antidepressant drugs amitriptyline and imipramine. Farmaco 55(3):211–218
5. Serafeim A, Holder MJ, Grafton G, Chamba A, Drayson MT, Luong QT, Bunce CM, Gregory CD et al (2003) Selective serotonin reuptake inhibitors directly signal for apoptosis in biopsy-like Burkitt lymphoma cells. Blood 101(8):3212–3219. https://doi.org/10.1182/blood-2002-07-2044
6. Cordero MD, Sanchez-Alcazar JA, Bautista-Ferrufino MR, Carmona-Lopez MI, Illanes M, Rios MJ, Garrido-Maraver J, Alcudia A et al (2010) Acute oxidant damage promoted on cancer cells by amitriptyline in comparison with some common chemotherapeutic drugs. Anti-Cancer Drugs 21(10):932–944. https://doi.org/10.1097/CAD.0b013e32833ed5f7
7. Lirk P, Haller I, Hausott B, Ingorokva S, Deibl M, Gerner P, Klimaschewski L (2006) The neurotoxic effects of amitriptyline are mediated by apoptosis and are effectively blocked by inhibition of caspase activity. Anesth Analg 102(6):1728–1733. https://doi.org/10.1213/01.ane.0000216018.62549.bb
8. Lee MY, Hong S, Kim N, Shin KS, Kang SJ (2015) Tricyclic antidepressants amitriptyline and desipramine induced neurotoxicity associated with Parkinson's disease. Mol Cells 38(8):734–740. https://doi.org/10.14348/molcells.2015.0131
9. Slamon ND, Ward TH, Butler J, Pentreath VW (2001) Assessment of DNA damage in C6 glioma cells after antidepressant treatment using an alkaline comet assay. Arch Toxicol 75(4):243–250
10. Hassanane MS, Hafiz N, Radwan W, El-Ghor AA (2012) Genotoxic evaluation for the tricyclic antidepressant drug, amitriptyline. Drug Chem Toxicol 35(4):450–455. https://doi.org/10.3109/01480545.2011.642382
11. Needham BL, Mezuk B, Bareis N, Lin J, Blackburn EH, Epel ES (2015) Depression, anxiety and telomere length in young adults: evidence from the National Health and nutrition examination survey. Mol Psychiatry 20(4):520–528. https://doi.org/10.1038/mp.2014.89
12. Dubal DB, Zhu L, Sanchez PE, Worden K, Broestl L, Johnson E, Ho K, Yu GQ et al (2015) Life extension factor klotho prevents mortality and enhances cognition in hAPP transgenic mice. J Neurosci 35(6):2358–2371. https://doi.org/10.1523/JNEUROSCI.5791-12.2015
13. Dubal DB, Yokoyama JS, Zhu L, Broestl L, Worden K, Wang D, Sturm VE, Kim D et al (2014) Life extension factor klotho enhances cognition. Cell Rep 7(4):1065–1076. https://doi.org/10.1016/j.celrep.2014.03.076
14. Zeldich E, Chen CD, Colvin TA, Bove-Fenderson EA, Liang J, Tucker Zhou TB, Harris DA, Abraham CR (2014) The neuroprotective effect of klotho is mediated via regulation of members of the redox system. J Biol Chem 289(35):24700–24715. https://doi.org/10.1074/jbc.M114.567321
15. German DC, Khobahy I, Pastor J, Kuro OM, Liu X (2012) Nuclear localization of klotho in brain: An anti-aging protein. Neurobiol Aging 33(7):1483 e1425–1483 e1430. https://doi.org/10.1016/j.neurobiolaging.2011.12.018
16. Mytych J, Wos I, Solek P, Koziorowski M (2017) Protective role of klotho protein on epithelial cells upon co-culture with activated or senescent monocytes. Exp Cell Res 350(2):358–367. https://doi.org/10.1016/j.yexcr.2016.12.013
17. Mytych J, Lewinska A, Bielak-Zmijewska A, Grabowska W, Zebrowski J, Wnuk M (2014) Nanodiamond-mediated impairment of nucleolar activity is accompanied by oxidative stress and DNMT2 upregulation in human cervical carcinoma cells. Chem Biol Interact 220:51–63. https://doi.org/10.1016/j.cbi.2014.06.004
18. O'Callaghan NJ, Fenech M (2011) A quantitative PCR method for measuring absolute telomere length. Biol Proced Online 13:3. https://doi.org/10.1186/1480-9222-13-3
19. Solek P, Majchrowicz L, Koziorowski M (2018) Aloe arborescens juice prevents EMF-induced oxidative stress and thus protects from pathophysiology in the male reproductive system in vitro. Environ Res 166:141–149. https://doi.org/10.1016/j.envres.2018.05.035
20. Pampalona J, Soler D, Genesca A, Tusell L (2010) Telomere dysfunction and chromosome structure modulate the contribution of individual chromosomes in abnormal nuclear morphologies. Mutat Res 683(1–2):16–22. https://doi.org/10.1016/j.mrfmmm.2009.10.001
21. Brobey RK, German D, Sonsalla PK, Gurnani P, Pastor J, Hsieh CC, Papaconstantinou J, Foster PP et al (2015) Klotho protects dopaminergic neuron oxidant-induced degeneration by modulating ASK1 and p38 MAPK signaling pathways. PLoS One 10(10):e0139914. https://doi.org/10.1371/journal.pone.0139914
22. Hsieh HJ, Liu CA, Huang B, Tseng AH, Wang DL (2014) Shear-induced endothelial mechanotransduction: the interplay between reactive oxygen species (ROS) and nitric oxide (NO) and the pathophysiological implications. J Biomed Sci 21:3. https://doi.org/10.1186/1423-0127-21-3
23. Zhang Y, Wang H, Li J, Jimenez DA, Levitan ES, Aizenman E, Rosenberg PA (2004) Peroxynitrite-induced neuronal apoptosis is mediated by intracellular zinc release and 12-lipoxygenase activation. J Neurosci 24(47):10616–10627. https://doi.org/10.1523/JNEUROSCI.2469-04.2004
24. Six I, Okazaki H, Gross P, Cagnard J, Boudot C, Maizel J, Drueke TB, Massy ZA (2014) Direct, acute effects of klotho and FGF23 on vascular smooth muscle and endothelium. PLoS One 9(4):e93423. https://doi.org/10.1371/journal.pone.0093423
25. Vincent SR (2010) Nitric oxide neurons and neurotransmission. Prog Neurobiol 90(2):246–255. https://doi.org/10.1016/j.pneurobio.2009.10.007
26. Parween S, Varghese DS, Ardah MT, Prabakaran AD, Mensah-Brown E, Emerald BS, Ansari SA (2017) Higher O-GlcNAc levels are associated with defects in progenitor proliferation and premature neuronal differentiation during in-vitro human embryonic cortical neurogenesis. Front Cell Neurosci 11:415. https://doi.org/10.3389/fncel.2017.00415
27. Liu C, Li J (2018) O-GlcNAc: A sweetheart of the cell cycle and DNA damage response. Front Endocrinol (Lausanne) 9:415. https://doi.org/10.3389/fendo.2018.00415
28. Diotti R, Loayza D (2011) Shelterin complex and associated factors at human telomeres. Nucleus 2(2):119–135. https://doi.org/10.4161/nucl.2.2.15135
29. Takai H, Smogorzewska A, de Lange T (2003) DNA damage foci at dysfunctional telomeres. Curr Biol 13(17):1549–1556
30. Opresko PL, Fan J, Danzy S, Wilson DM 3rd, Bohr VA (2005) Oxidative damage in telomeric DNA disrupts recognition by TRF1 and TRF2. Nucleic Acids Res 33(4):1230–1239. https://doi.org/10.1093/nar/gki273
31. Kim SH, Davalos AR, Heo SJ, Rodier F, Zou Y, Beausejour C, Kaminker P, Yannone SM et al (2008) Telomere dysfunction and cell survival: roles for distinct TIN2-containing complexes. J Cell Biol 181(3):447–460. https://doi.org/10.1083/jcb.200710028
32. Kelleher C, Kurth I, Lingner J (2005) Human protection of telomeres 1 (POT1) is a negative regulator of telomerase activity in vitro. Mol Cell Biol 25(2):808–818. https://doi.org/10.1128/MCB.25.2.808-818.2005

33. Verdun RE, Crabbe L, Haggblom C, Karlseder J (2005) Functional human telomeres are recognized as DNA damage in G2 of the cell cycle. Mol Cell 20(4):551–561. https://doi.org/10.1016/j.molcel.2005.09.024
34. Fang KM, Liu JJ, Li CC, Cheng CC, Hsieh YT, Chai KM, Lien YA, Tzeng SF (2015) Colchicine derivative as a potential anti-glioma compound. J Neuro-Oncol 124(3):403–412. https://doi.org/10.1007/s11060-015-1874-2
35. Balmer D, Emery M, Andreux P, Auwerx J, Ginet V, Puyal J, Schorderet DF, Roduit R (2013) Autophagy defect is associated with low glucose-induced apoptosis in 661W photoreceptor cells. PLoS One 8(9):e74162. https://doi.org/10.1371/journal.pone.0074162
36. Gewirtz DA (2014) The four faces of autophagy: implications for cancer therapy. Cancer Res 74(3):647–651. https://doi.org/10.1158/0008-5472.CAN-13-2966
37. Hung HH, Huang WP, Pan CY (2013) Dopamine- and zinc-induced autophagosome formation facilitates PC12 cell survival. Cell Biol Toxicol 29(6):415–429. https://doi.org/10.1007/s10565-013-9261-2
38. Whitwell J, Smith R, Jenner K, Lyon H, Wood D, Clements J, Aschcroft-Hawley K, Gollapudi B et al (2015) Relationships between p53 status, apoptosis and induction of micronuclei in different human and mouse cell lines in vitro: Implications for improving existing assays. Mutat Res Genet Toxicol Environ Mutagen 789-790:7–27. https://doi.org/10.1016/j.mrgentox.2015.05.011
39. Xu F, Li X, Yan L, Yuan N, Fang Y, Cao Y, Xu L, Zhang X et al (2017) Autophagy promotes the repair of radiation-induced DNA damage in bone marrow hematopoietic cells via enhanced STAT3 signaling. Radiat Res 187(3):382–396. https://doi.org/10.1667/RR14640.1
40. Zhou WJ, Deng R, Zhang XY, Feng GK, Gu LQ, Zhu XF (2009) G-quadruplex ligand SYUIQ-5 induces autophagy by telomere damage and TRF2 delocalization in cancer cells. Mol Cancer Ther 8(12):3203–3213. https://doi.org/10.1158/1535-7163.MCT-09-0244
41. Zschocke J, Zimmermann N, Berning B, Ganal V, Holsboer F, Rein T (2011) Antidepressant drugs diversely affect autophagy pathways in astrocytes and neurons–dissociation from cholesterol homeostasis. Neuropsychopharmacology 36(8):1754–1768. https://doi.org/10.1038/npp.2011.57